

# Tuning of nanocavity optomechanical coupling using a near-field fiber probe: supplementary material

AARON C. HRYCIW<sup>1</sup>, MARCELO WU<sup>2,3</sup>, BEHZAD KHANALILOO<sup>2,3</sup>, AND PAUL E. BARCLAY<sup>2,3,\*</sup>

<sup>1</sup>nanoFAB Facility, University of Alberta, Edmonton, AB, T6G 2R3, Canada

<sup>2</sup>National Institute for Nanotechnology, Edmonton, AB, T6G 2M9, Canada

<sup>3</sup>Institute for Quantum Science and Technology, University of Calgary, Calgary, AB, T2N 1N4, Canada

\*Corresponding author: pbarclay@ucalgary.ca

Published 14 May 2015

This document provides supplementary information to "Near-field tuning of optomechanical coupling in a split-beam nanocavity," <http://dx.doi.org/10.1364/optica.2.000491>. The relative contribution of dispersive vs. dissipative optomechanical coupling in a nanophotonic "split-beam" cavity (SBC) can be tuned by using an optical fiber taper to perturb the cavity's optical near field. First, we briefly describe a model for optomechanical coupling between a fiber and a cavity which includes both dispersive and dissipative transduction. Next, we discuss in more detail the assumptions used in our numerical simulations of the external dissipative optomechanical coupling coefficient,  $g_e$ . We further present perturbative approximations for  $g_{om}$  and  $g_e$ , by way of elucidating the principal physical processes which give rise to the optomechanical transduction observed in the fiber-cavity system. Finally, we show how the dissipative–dispersive coupling transition can also be effected via translating the fiber along the nanobeam axis with fixed height. © 2015 Optical Society of America

<http://dx.doi.org/10.1364/optica.2.000491.s001>

## 1. DISPERSIVE AND DISSIPATIVE OPTOMECHANICAL COUPLING

In the following, we present a simplified model for fiber–cavity coupling in the sideband-unresolved regime, taking into account both dissipative and dispersive optomechanical coupling; a more complete discussion may be found in Appendix 1 of Ref. [1].

We consider an optical fiber taper placed in the near field of an optical cavity with resonance frequency  $\omega_o$ . Input light from the fiber couples to the cavity, with the transmitted signal in the fundamental fiber mode being measured by a photodetector. The loss channels for the cavity are: 1) coupling into the forward- or backward-propagating modes of the fiber, each described by a rate of  $\gamma_e$ , and 2) intrinsic cavity loss ( $\gamma_i$ ) and fiber-induced parasitic loss ( $\gamma_p$ ), which we describe collectively by a rate of  $\gamma_{i+p} = \gamma_i + \gamma_p$ . In the main text,  $Q_i$  also includes parasitic loss such that  $Q_i \rightarrow Q_{i+p}$ .

For weak fiber–cavity coupling, in which  $\gamma_e \ll \gamma_{i+p}$ , the

transmission spectrum of the fiber may be written as [1]

$$T \sim \frac{\Delta^2 + \left(\frac{\gamma_{i+p}}{2}\right)^2}{\Delta^2 + \left(\frac{\gamma_t}{2}\right)^2}, \quad (\text{S1})$$

where  $\Delta = \omega_l - \omega_o$  is the detuning of the input laser with respect to the cavity resonance,  $\gamma_t = \gamma_{i+p} + 2\gamma_e$  is the total cavity optical loss rate, and we have neglected a Fano modification to the cavity response brought about by coupling to higher-order fiber modes that are converted to the fundamental fiber mode.

The cavity's optomechanical response with respect to a supported mechanical mode of frequency  $\omega_m$  may be thought of as stemming from the effect of the global amplitude of the motion,  $x$ , on the parameters in Eq. (S1). In the sideband-unresolved/"bad-cavity" regime ( $\omega_m \ll \gamma_t$ ), the fiber transmission adiabatically follows the mechanical oscillation [2], such that a mechanical displacement  $dx$  yields a correspond-

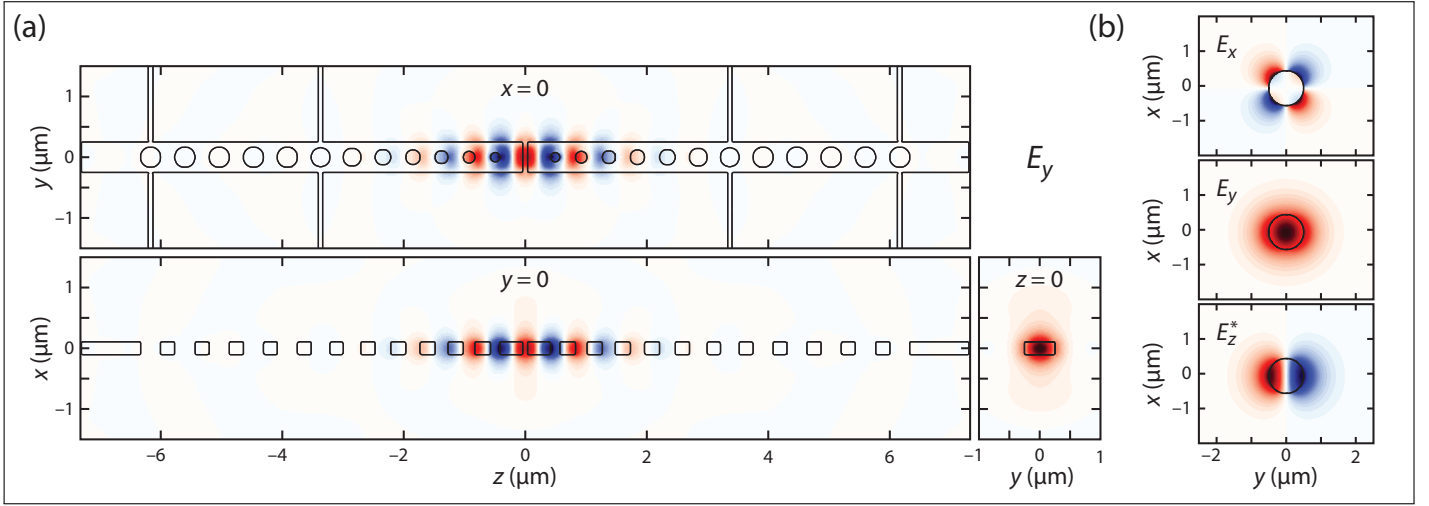


**Fig. S1.** Unperturbed electric field profiles of the fundamental TE-like mode of (a) the split-beam cavity ( $E_y$  only) and (b) a 1- $\mu\text{m}$ -diameter fiber

ing change in transmission given by

$$\frac{dT}{dx}(\Delta) = \left| g_{\text{om}} \frac{\partial T}{\partial \Delta} + g_i \frac{\partial T}{\partial \gamma_{i+p}} + g_e \frac{\partial T}{\partial \gamma_e} \right|. \quad (\text{S2})$$

In the above,  $g_{\text{om}} = d\omega_o/dx$ ,  $g_i = d\gamma_{i+p}/dx$ , and  $g_e = d\gamma_e/dx$  are the dispersive, intrinsic dissipative, and external dissipative optomechanical coupling coefficients, respectively [1].

Differentiating Eq. (S1) with respect to each of its parameters yields

$$\frac{\partial T}{\partial \Delta} = \frac{2\Delta(1-T)}{\Delta^2 + (\gamma_t/2)^2} \quad (\text{S3})$$

$$\frac{\partial T}{\partial \gamma_{i+p}} = \frac{\gamma_{i+p} - T(\gamma_{i+p} + 2\gamma_e)}{\Delta^2 + (\gamma_t/2)^2} \quad (\text{S4})$$

$$\frac{\partial T}{\partial \gamma_e} = \frac{-2\gamma_e T}{\Delta^2 + (\gamma_t/2)^2}. \quad (\text{S5})$$

We may then compare the contribution of these terms to the  $S_{\text{VV}}(\lambda)$  lineshape by considering their peak amplitudes [2]:

$$\left. \frac{\partial T}{\partial \Delta} \right|_{\text{max}} = \frac{dT}{d\Delta}(\Delta = \frac{\gamma_t}{2}) = (1 - T_d) \frac{Q_o}{\omega_o} \quad (\text{S6})$$

$$\left. \frac{\partial T}{\partial \gamma_{i+p}} \right|_{\text{max}} = \frac{dT}{d\gamma_{i+p}}(\Delta = 0) = 4(1 - T_d) \frac{Q_o}{\omega_o} \quad (\text{S7})$$

$$\left. \frac{\partial T}{\partial \gamma_e} \right|_{\text{max}} = \frac{dT}{d\gamma_e}(\Delta = 0) = -8T_d \frac{Q_o}{\omega_o} \quad (\text{S8})$$

where  $T_d = \gamma_{i+p}^2/\gamma_t^2$  is the on-resonance transmission depth and  $Q_o = \omega_o/\gamma_t$  is the optical quality factor; note that the maxima in these derivatives do not all occur at the same detuning  $\Delta$ . For weak fiber-nanocavity coupling ( $1 - T_d \ll 1$ )<sup>1</sup>, and for the mechanical modes with minimal intrinsic dissipative optomechanical coupling ( $d\gamma_i/dx \ll d\gamma_e/dx$ ), as in the system studied here, the dissipative contribution to the measured optomechanical signal is dominated by  $\gamma_e$  [1]. As such, we express

<sup>1</sup>Note that in this regime contributions to the optomechanical signal from  $d\gamma_p(x)/dx$  will be small compared to  $d\gamma_e(x)/dx$  if  $|d\gamma_p/dx| \leq |d\gamma_e/dx|$ .

the relative balance of experimentally observed dissipative and dispersive signal by the ratio  $\Gamma$  given in the main text:

$$\Gamma = \left| \frac{g_e \frac{dT}{d\gamma_e} \Big|_{\text{max}}}{g_{\text{om}} \frac{dT}{d\omega_o} \Big|_{\text{max}}} \right| = \frac{8g_e T_d}{g_{\text{om}}(1 - T_d)}. \quad (\text{S9})$$

## 2. FEA ESTIMATE OF $g_e$

The system under study is a fiber-nanocavity system in which the distance  $h$  changes the coupling rate  $\gamma_e(h)$  between the cavity and both the forward- and backward-propagating waves of the fiber as illustrated in Fig. 1(b) of the main text. Here  $h$  is defined as the distance between the nanocavity and the outer boundary of the fiber. The presence of the fiber may also create other loss channels by scattering light away from the fiber or by coupling to higher-order waveguide modes. These are bundled together as parasitic loss rate  $\gamma_p(h)$  [3]. The nanocavity itself has a radiation loss rate of  $\gamma_{\text{rad}}$ , which can be computed via numerical simulations (FDTD, FEA), and a scattering loss rate  $\gamma_s$  due to fabrication imperfections. Together, they form the intrinsic loss of the nanocavity:  $\gamma_i = \gamma_{\text{rad}} + \gamma_s$ . The total loss rate  $\gamma_t$  is then given by

$$\gamma_t(h) = \gamma_i + \gamma_p(h) + 2\gamma_e(h). \quad (\text{S10})$$

To generate the theoretical values for  $g_e(h)$ , and hence  $T_d(h)$  and  $\Gamma(T_d, g_e, g_{\text{om}})$ , used in Fig. 4 of the main text,  $\gamma_e(h)$  was estimated from FEA (COMSOL) simulations of  $\gamma_t(h)$ . This was done by extracting  $Q_o(h)$  while translating the fiber vertically above the (stationary) nanobeam. Since this method does not exactly model the mechanical mode displacement, the values extracted are only an approximation. Precisely determining  $\gamma_e(h)$  given  $\gamma_t(h)$  requires knowledge of  $\gamma_p(h)$ . Here, we assess  $\gamma_p$  based on experimentally observed  $T_d(h=0)$  and  $\gamma_i = \gamma_t(h \rightarrow \infty)$ , from which the ratio  $\gamma_e(0)/(\gamma_e(0) + \gamma_p(0)) = 0.4$  was extracted. Making the simplifying assumption that  $\gamma_e/(\gamma_e + \gamma_p)$  is constant for all  $h$  allows an estimate of  $\gamma_e(h)$  to be determined from the simulated values of  $\gamma_t(h)$ .

This procedure likely overestimates  $\gamma_p$  for  $h > 0$ , as  $\gamma_p$  typically decays with  $h$  quickly compared to  $\gamma_e$ , i.e. the coupling becomes more ideal as  $h$  increases [3]. As a result, this procedure may underestimate  $\gamma_e$  for large  $h$ , and underestimate the decay

constant  $\Lambda_e$  of  $g_e$ . However, the key features in Figure 5, notably that  $\Lambda_e > \Lambda_{om}$ , and that  $\Gamma = 1$  when  $h \sim 300$  nm, are not found to be significantly affected by these uncertainties.

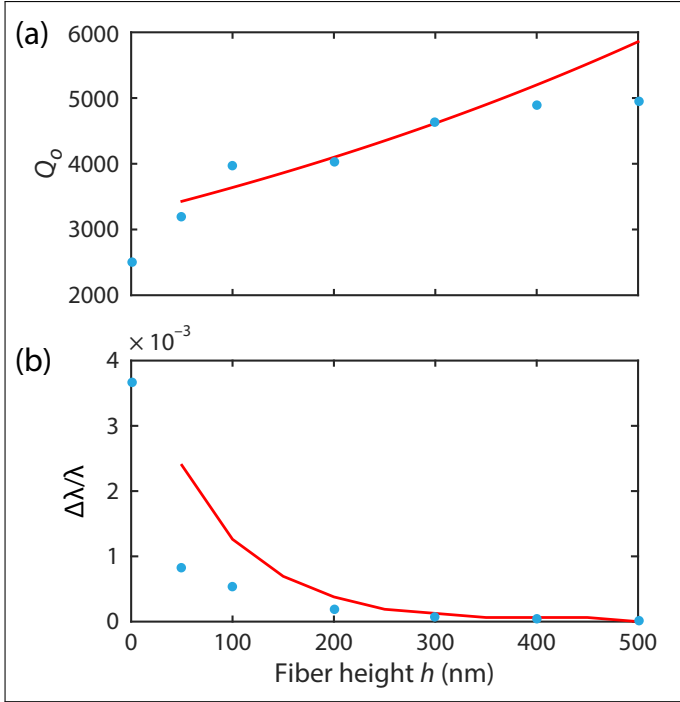


**Fig. S2.** Comparison between simulated (red line) and experimental (blue circles) values of (a) optical quality factor  $Q_0$  and (b) shift in wavelength  $\Delta\lambda/\lambda$  at various fiber heights when hovering above M2 ( $z_f = 2 \mu\text{m}$ ).

Figures S2(a) and (b) show experimental and FEA-simulated values for the optical quality factor  $Q_0$  and the shift in wavelength  $\Delta\lambda/\lambda$ , respectively, of the cavity resonance. The good agreement in  $Q_0$  gives confidence in our approximation of  $g_e$ . The smaller shift in wavelength observed in our experiments compared to simulations could correlate to the lower  $g_{om}$  values in Fig. 5(a).

In principle,  $\gamma_p(h)$  could be measured experimentally; however, this was difficult in the system under study due to the relatively small  $h < 500$  nm at which coupling was observed (resulting in significant fiber taper insertion loss) and the poor contrast of the measured nanocavity resonance. In future, fabrication of nanocavities with higher  $Q_0$  may address this difficulty.

### 3. PERTURBATIVE APPROXIMATIONS FOR $g_{om}$ AND $g_e$

To gain insight into the physical mechanisms governing the effect of the fiber taper on  $g_{om}$  and  $g_e$ , we evaluate the shift in cavity resonance frequency,  $\omega_0$ , and coupling rate between the fiber and cavity,  $\gamma_e$ , using first-order perturbation theory.

#### A. Unperturbed cavity and fiber fields

The unperturbed cavity field  $\mathbf{E}_c$ , the dominant  $y$ -component of which is shown in Fig. S1(a), was calculated using FDTD simulations [4] of the cavity geometry as determined from SEM images of the device. The dielectric profile of the cavity,  $\epsilon_c(\mathbf{r})$ , is assumed to have inversion symmetry; in particular, the circular hole radii and positions are specified to be symmetric with respect to the  $z = 0$  plane. The fundamental TE-like cavity

mode ( $E$ -field even in  $x$ , odd in  $y$ ) has a resonance wavelength of  $\sim 1612$  nm, a quality factor of  $1.2 \times 10^4$  (limited by scattering in the  $x$  and  $y$  directions), and an effective mode volume of  $\sim 0.35 (\lambda/n)^3$ .

The unperturbed fiber taper fields were calculated using a frequency-domain eigenmode solver [5], assuming a  $\text{SiO}_2$  ( $n_f = 1.44$ ) fiber with a diameter of  $1 \mu\text{m}$  in air. This fiber supports a single TE-like mode at a wavelength of  $1612$  nm, with a propagation constant  $\beta = 4.5 \mu\text{m}^{-1}$ .

#### B. Cavity resonant frequency

The first-order correction to the resonant frequency of an electromagnetic cavity due to a change in permittivity may be calculated using [6]

$$\Delta\omega_0 = -\frac{\omega_0}{2} \frac{\langle \mathbf{E}_c | \Delta\epsilon_f | \mathbf{E}_c \rangle}{\langle \mathbf{E}_c | \epsilon_c | \mathbf{E}_c \rangle}, \quad (\text{S11})$$

where  $\mathbf{E}_c$  and  $\omega_0$  are the unperturbed cavity electric field and resonant frequency, respectively,  $\Delta\epsilon_f$  is the perturbation of the local dielectric environment due to the fiber, and  $\langle \rangle$  represents integration over all space. For the geometry considered in this paper,  $\Delta\epsilon_f = \epsilon_f - 1$ , with the integral restricted to the region inside the fiber taper. As in the finite-element calculations in Fig. 4(a) of the main text, we model a dimpled fiber with a  $25 \mu\text{m}$  radius of curvature (see inset to Fig. S3).

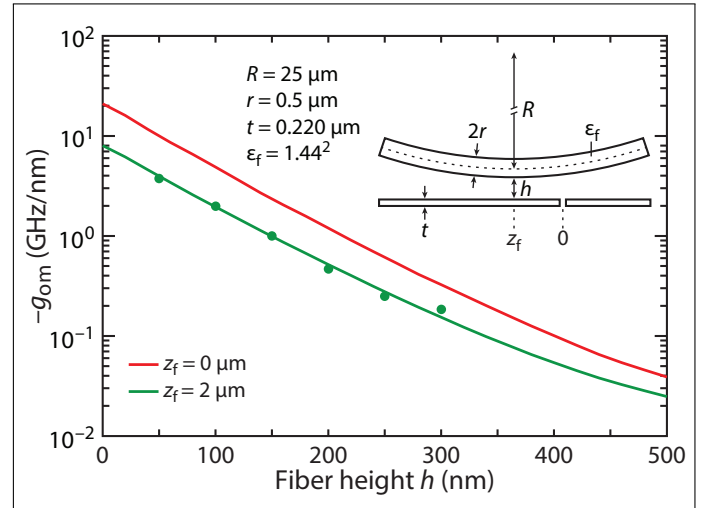


**Fig. S3.** Dispersive coupling coefficient  $g_{om}$  calculated using first-order perturbation theory; the simulation geometry is shown in the inset. The red (green) line corresponds to an axial fiber offset  $z_f$  of  $0$  ( $-2$ )  $\mu\text{m}$  from the cavity center. The green circles are the  $g_{om,M1}$  values from Fig. 4(a) of the main text, calculated using FEA.

From this expression, we see that the change in the cavity resonant frequency with  $h$  scales with the intensity of the evanescent cavity field overlapping with the fiber. For a cantilever mode,  $dx \equiv -dh$ , such that  $g_{om} \sim -\frac{d\Delta\omega_0}{dh}$  decays with the same quasi-exponential dependence. Fig. S3 plots  $g_{om}$  using this approach for the dimple centered on the cavity ( $z_f = 0 \mu\text{m}$ ) and offset axially over one of the mirrors ( $z_f = -2 \mu\text{m}$ ); the latter agrees well with  $g_{om}$  calculated using FEA for the full fiber-cavity system, as shown in Fig. 4(a) of the main text.

### C. Fiber–cavity coupling

An approximation for the cavity loss rate into the fiber,  $\gamma_e$ , can be obtained from coupling-mode analysis for a generalized waveguide–resonator system [7]. Neglecting dispersion, the loss rate into either the forward- or backward-propagating fiber mode is

$$\gamma_e = \left| \frac{\omega \epsilon_0}{4} \int_{z_1}^{z_2} dz \iint dx dy (\epsilon_c - 1) \mathbf{E}_c^* \cdot \mathbf{E}_f e^{-i\beta z} \right|^2, \quad (\text{S12})$$

where  $\epsilon_c$  is the relative permittivity of the cavity,  $\mathbf{E}_c(x, y, z)$  is the unperturbed cavity electric field distribution (normalized to unit energy),  $\mathbf{E}_f(x, y)$  is the unperturbed fiber electric field mode profile (normalized to unit power),  $\beta$  is the fiber mode propagation constant, and the integrals in  $x$  and  $y$  are restricted to the region inside the cavity dielectric. As a simple approximation for the effect of the dimple curvature, we assume a straight fiber at a distance  $h$  above the cavity and integrate over an effective coupling length  $\Delta z$  centered at  $z_f$  (i.e.,  $z_1 = z_f - \frac{\Delta z}{2}$ ,  $z_2 = z_f + \frac{\Delta z}{2}$ ). Assuming  $dx > 0$  corresponds to deflection of the cantilever toward the fiber, then for a fiber–cavity separation  $h$ , we then have  $g_e \sim -\frac{d\gamma_e}{dh}$ . Fig. S4(a) plots  $g_e$  calculated via this approach for dimple center positions  $z_f$  of 0 and  $-2 \mu\text{m}$ .

Note that  $g_e$  calculated using this approach does not take into account contributions from coupling to higher-order fiber modes that are converted to the fundamental mode, which may in part explains its lower magnitude with respect to the calculation shown in Fig. 4(a) of the main text, and as explained in §2 above. Although this treatment is approximate, it captures several features of the full FEA approach, including non-monotonic behavior of  $g_e(h)$  with  $z_f = 0 \mu\text{m}$  for certain coupling lengths (Fig. S4(c), top), and sensitivity of the magnitude of  $g_e$  (Fig. S4(a)) and its decay length  $\Lambda_e$  (Fig. S4(b)) to dimple position  $z_f$ . The richer physics of this coupling mechanism compared with  $g_{\text{om}}$  may be traced to its origin as an interference effect, which does not enter into the dispersive coupling calculation.

### 4. DISSIPATIVE–DISPERSIVE COUPLING TRANSITION VIA AXIAL FIBER MOTION

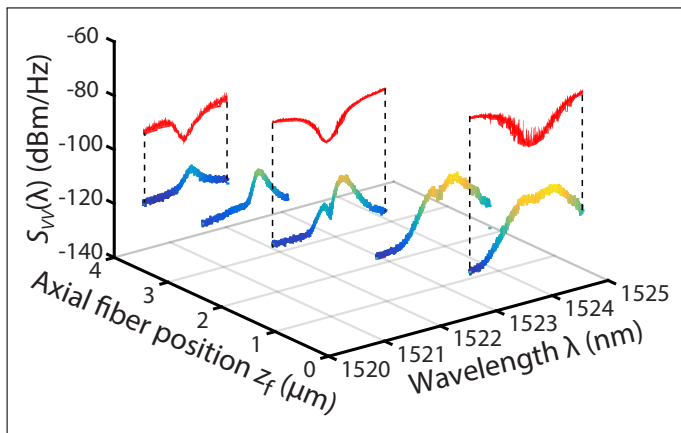


**Fig. S5.**  $S_{VV}$  vs.  $\lambda$  for varying axial fiber positions  $z_f$  along the nanobeam. The fiber is hovering about  $h = 100 \text{ nm}$  above M2. At  $z = 0$ , the fiber dimple is directly above the center of the cavity.  $T(\lambda)$  in red is shown for selected heights.

As demonstrated in the main text, the presence of the fiber affects both the strength and the dispersive/dissipative charac-

ter of the optomechanical signal. With the fiber taper dimple aligned with the center of the SBC, a transition from predominantly dissipative to dispersive coupling is observed as the fiber moves vertically toward the nanobeam, as illustrated in Fig. 4(b). A complementary measurement further demonstrating this effect is to monitor the optomechanical signal while moving the dimple along the nanobeam axis ( $z$  direction). When the fiber taper is far from the center of the cavity, shown on the left in Fig. S5, the optomechanical coupling is strongly dissipative in nature. As the fiber moves toward the central gap where the field is concentrated, its influence increases and  $g_{\text{om}}$  becomes dominant by  $z_f = 2 \mu\text{m}$ . However, at very close proximity to the center of the cavity ( $z_f \leq 1 \mu\text{m}$ ), both the optical resonance and the optomechanical signal become unstable due to the near-field disturbance of the fiber. This is evident in the noisy nature of the fiber taper transmission, and the low visibility of the “zero” in the optomechanical response.

### REFERENCES

1. M. Wu, A. C. Hryciw, C. Healey, D. P. Lake, H. Jayakumar, M. R. Freeman, J. P. Davis, and P. W. Barclay, *Phys. Rev. X* (2014).
2. A. G. Krause, M. Winger, T. D. Blasius, W. Lin, and O. Painter, *Nat. Photon.* **6**, 768 (2012).
3. S. M. Spillane, T. J. Kippenberg, O. J. Painter, and K. J. Vahala, *Phys. Rev. Lett.* **91**, 043902 (2003).
4. A. F. Oskooi, D. Roundy, M. Ibanescu, P. Bermel, J. Joannopoulos, and S. G. Johnson, *Comp. Phys. Comm.* **181**, 687 (2010).
5. S. Johnson and J. Joannopoulos, *Optics Express* **8**, 173 (2001).
6. S. G. Johnson, M. Ibanescu, M. A. Skorobogatiy, O. Weisberg, J. D. Joannopoulos, and Y. Fink, *Phys. Rev. E* **65**, 066611 (2002).
7. C. Manolatou, M. J. Khan, S. Fan, P. R. Villeneuve, H. A. Haus, and J. D. Joannopoulos, *IEEE J. Quantum Electron.* **35**, 1322 (1999).

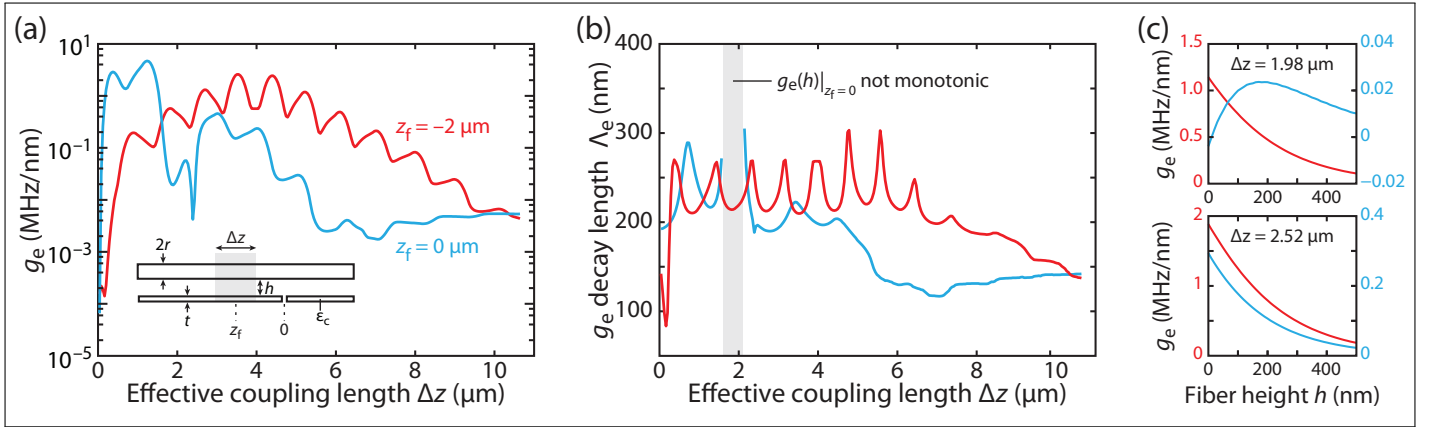


**Fig. S4.** Dissipative coupling coefficient  $g_e$  calculated from mode-coupling theory for a fiber height of 200 nm; the simulation geometry is shown in the inset to (a), where the grey box denotes the integration limits on  $z$ . In all cases, blue (red) corresponds to a  $z_f$  of 0 ( $-2$ )  $\mu\text{m}$ . (a)  $g_e$  as a function of effective coupling length. (b) Decay lengths obtained from single-exponential fits of  $g_e(h)$ . (c)  $g_e$  vs.  $h$  for coupling lengths of 1.98  $\mu\text{m}$  (top) and 2.52  $\mu\text{m}$  (bottom).